https://erjm.journals.ekb.eg
ISSN: 1110-1180

DOI: ---------

ERJ
Engineering Research Journal
Faculty of Engineering
Menoufia University

Improving the Dynamic Performance of the Crank-Rocker Mechanism Using Composite Links

Mamdouh I. Elamy[1,2]

[1]*Industrial Engineering Department, College of Engineering, Northern Border University, Arar, Saudi Arabia. On leave from*
[2]*Department of Production Engineering & Mechanical Design, Faculty of Engineering, University of Menoufia, Shebin El-kom, Menoufia, Egypt.*
mamdouhelimi2017@gmail.com, Mamdouh.Morsi@nbu.edu.sa

ABSTRACT

In practice, the transmission angle is a crucial factor for reducing the required driving power and improving the dynamic performance of the mechanisms and machines. The vibration of elastic links is unavoidable in mechanisms running at high speeds. Thus, optimum link lengths decrease driving power since they ensure optimal transmission angles. In addition, joints made of hybrid and nonhybrid composites are lightweight and require less driving torque. Additionally, composite links can be used in place of metal links to alleviate wear and corrosion issues. Through the use of composite links, the dynamic performance of the mechanism and the machine will be improved as a result of the higher damping factor, stiffness, and flexural modulus values of the composite materials. Accordingly, this research considers the effect of transmission angle, four case types of linkages proportions, and stacking sequences on the natural frequencies and instability thresholds of the mechanisms. Therefore, the finite element method (FEM) was used to efficiently compute the Eigen-nature for the mechanisms with composite links. The experimental tests are also conducted using the frequency response function method (FRF). Based on the results, the CR mechanism performs best at 90° of the transmission angle, as the average natural frequency of this angle decreases by 11.19 % and 26.17 % compared to the maximum and minimum transmission angles. Overall, the measuring and theoretical fundamental response frequencies of mechanisms are in good agreement.

Keywords:*Transmission angle, Finite element analysis, Composite materials*

1. Introduction

The four-bar planar mechanism is the most commonly used in mechanical systems. A crank-rocker (CR) mechanism is a popular type of planar oscillatory mechanism. Over the past few decades, more research has been conducted on CR mechanism design. This design considers unit time ratios and minimum transmission angles, as presented by J. Brodell et al. [1] more than 60 years ago, while the CR mechanism design related to the human knee exoskeletons was reported in [2].

Couplers and followers are connected by a smaller angle called the transmission angle. Further, the transmission angle is equal to the angle formed between the two velocity vectors at the connection pivot, as discussed in [3-8]. The transmission angle significantly contributes to improving the dynamic characteristics of CR. Moreover, the transmission angles have a significant effect on the smooth operation of the CR mechanism.

In general, minimal driving torque fluctuations, an acceptable transmission angle, smooth transmission motion, low-pressurized bearing movements, and low vibrations are the goals of all mechanism designers. Most of the potential problems associated with the CR mechanism can be addressed using the optimal transmission angles, as described by S. Balli et al. [5]. As discussed in [9], too big or too small transmission angles are always associated with undesirable noise. A big transmission angle is also insufficient to maintain low variations of the driving torque.

Optimizing mechanism linkages is, unfortunately, a complex problem, especially when considering transmission characteristics and simultaneously synthesizing the mechanism's transmission angle. Nevertheless, as mentioned in [10], this problem can be significantly simplified by considering a limited transmission angle range identified by two specific values.

The minimum and maximum transmission angles are affected by the rocker link's oscillation angle. Furthermore, Eschenbach et al [11] suggest that a reasonable transmission angle variation from 90° is essential for smooth motion and acceptable vibration levels at high speeds. Consequently, the transmission effectiveness is reduced if there is a large variation in the transmission angle. Moreover, CR mechanisms with big deviations of the transmission angle around 90° can produce undesired noise and jerks at high speeds, as discussed in [12].

Numerous recent research articles have been presented that synthesize the maximum and minimum transmission angles with definite values. As an illustration, [13] gave an analytical synthesis for figuring out the minimum and maximum transmission angles of CR mechanisms handling movement between two tiny places. Additionally, Patal [14] provided a way for synthesizing the four-bar mechanism's linkages utilizing a technique for generating polynomial functions in order to create precise values for the appropriate transmission angles. Furthermore, a method for synthesizing a four-bar mechanism with three consecutive coupler positions and a specific transmission angle range of less than 17° was presented in [15]. Moreover, a method for optimizing the path synthesis of CR mechanisms according to the optimal transmission angle has been introduced in [16].

According to the findings of K. Gupta [17], a new way of optimizing a four-bar mechanism is to use a new concept called the mini-max, which denotes the transmission angles that can be optimum when the limits are equal and around 90˚. Likewise, other reports have adopted the same mini-max sense, such as [18, 19]. Furthermore, definite transmission angle ranges as 35-145˚ and 30-150˚ are recommended in [20].

Several studies have also examined the modeling and analysis of 4-bar mechanisms to maximize output motion accuracy. Khan et al. [21] discussed the modeling and analysis of 4-bar mechanisms in automobiles. Dynamic analysis of rigid four-bar linkage has also been studied by Arda [22]. Lagrange's Equation has been used to determine the equation of motion, and the dynamic behavior of the four-bar linkage has been analyzed using MATLAB/Simulink.

In this paper, the dynamic performance of the four-bar mechanism was improved using hybrid and non-hybrid composite materials in addition to using four different cases of the mechanism, and three different types of transmission angles were studied. A frequency response function (FRF) method was used in the experimental analysis, which used an impact hammering test, while the numerical analysis used a finite element method (FEM).

2. Problem Formulation

Four-bar linkages are popular due to their simplicity and versatility in design. Moreover, since they are simple to manufacture, assemble, and maintain with few components and revolute joints, they can perform various tasks, including motion function and path generation. Accordingly, many designers prefer them over more complex linkages that perform the same tasks but more accurately [23].

The prototype of hybrid and non-hybrid composite linkages was handcrafted using glass and carbon fiber as strengthening mainstays in the form of bidirectional fabric and polyester with a catalyst as the matrix for the composite material. The laminated hybrid and non-hybrid composite links of crank-rocker mechanisms have a fiber volume fraction ratio of 60% in the same five layers of glass and carbon fiber as reinforcement.

Each link was made of five layers with various stacking sequences for each as set1: [C/C/C/C/C], set2: [C/C/G/C/C], set3: [C-G-C-G-C], set4: [G-C-G-C-G], set5: [G-G-C-G-G], set6: [G-G-G-G-G], at fiber volume fraction ratio is 60%. Where [C]: Carbon fiber and [G]: Glass fiber

An analytical calculation of mechanical properties is performed by utilizing the mixture rule. The mechanical properties of glass, carbon fiber, and polyester are listed in Table 1.

According to [24], Young's modulus (E), tensile strength (σ_{ult}), composite blade density (ρ), and the Poisson's ratio (ν_{xy}) are calculated analytically according to the mixture rule and specific theoretical equations, and their results are listed in Table 2.

Table 1. Mechanical properties of the used fibers and resin.

Utilized materials		Elasticity Modulus [GPa]	Shear Modulus [MPa]	Density [g/cm^3]	Poisson´s ratio
Reinforcement	E-Glass fiber	70±14	2400±4	2.580	0.20
	Carbon fiber	201.5 ±20	1526.5 ±642	1.74±0.01	0.210
Matrix	Polyester	2.43± 0.01	50.3±0.2	1.246± 0.01	0.350

Table 2. Results of mechanical properties of stacked composite links.

Stacking sequence	Laminate Codes	σ_{ult} (GPa)	E (GPa)	ν_{xy}	ρ (Kg/m^3)
[C-C-C-C-C]	C_1	99.73	2774.53	0.27	1538
[C-C-G-C-C]	C_2	92.24	2669.16	0.27	1640
[C-G-C-G-C]	C_3	84.25	2521.53	0.26	1742
[G-C-G-C-G]	C_4	73.32	2312.10	0.26	1844
[G-G-C-G-G]	C_5	66.60	2251.10	0.25	1946
[G-G-G-G-G]	C_6	62.61	2190.29	0.25	2048

2.1 Transmission Angle and its Limitations in Four-Bar Mechanism

The transmission angle γ is a smaller angle between the direction of the velocity difference vector of the driving link and the direction of the absolute velocity vector (V_C) of the output link, and both are taken at the point of connection, as shown in Fig. 1 [25]. It is the angle between the follower link and the coupler of a four-bar linkage.

These definitions are based on a joint variable, which is determined by the choice of driver and driven links. It appears to be an acute angle γ and an obtuse angle (180°-γ). It varies throughout the range of operation and is most favorable when it is 90°. The recommended transmission angle is 90 ±50°. In a mechanism with a motion reversal, if the roles of input and output links are reversed during the cycle, the transmission angle must be investigated for both directions of motion transmission.

Referring to the Fig. 1, the transmission angle in the form of an equation is given by Eq. (1) as follows:

$$\gamma = \cos^{-1}\frac{R_3^2+R_4^2-R_1^2-R_2^2+2R_1R_2\cos\theta_2}{2R_3R_4} \quad (1)$$

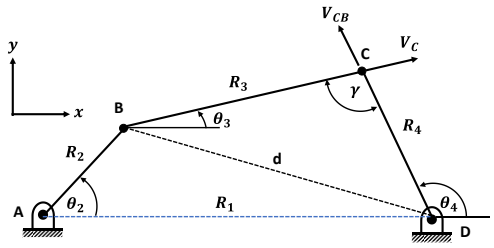

Figure 1- Transmission Angle

The motion of mechanism linkages becom impossible when the transmission angle is 0° or 180°. In the case of a zero-transmission angle, the output link cannot transfer torque, i.e., the mechanism is at its dead center. Moreover, low torque fluctuation is not guaranteed by a large transmission angle. If the transmission angle is too small or too large, the motion error will be large, the mechanism will be noisy, and it will be very prone to manufacturing errors [26].

2.2 Maximum and Minimum Transmission Angles

In the case of CR, the transmission angle will be minimum when the input crank angle is zero and will be maximum when the input crank angle is 180° (Fig. 2). These occur twice in each revolution of the driving crank, and they do not occur at the extreme positions of the linkage. Hence, both values of γ_{max} and γ_{min} can be formulated as presented in [27], according to Eqs. (2) and (3) as follows:

$$\gamma_{max} = \cos^{-1}\left[\frac{R_4^2+R_3^2-R_2^2-R_1^2-2R_1R_2}{2R_4R_3}\right] \quad (2)$$

$$\gamma_{min} = \cos^{-1}\left[\frac{R_4^2+R_3^2-R_2^2-R_1^2+2R_1R_2}{2R_4R_3}\right] \quad (3)$$

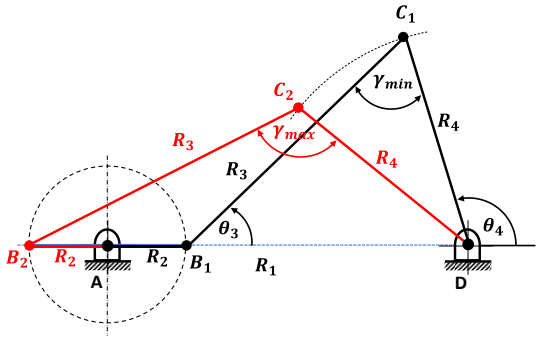

Figure 2 - Crank-Rocker Mechanism

A rocker link angle of θ_4 can also be calculated using the formula in Eq. (4), as introduced in [28] and associated with the CR geometry shown in Fig. 3.

$$\theta_4 = \begin{Bmatrix} \pi+\theta_1-\psi_1-\psi_3\,,\ where\quad \theta_1 \le \theta_2 < (\pi+\theta_1) \\ \pi+\theta_1+\psi_1-\psi_3\,,\ where\quad (\pi+\theta_1) \ge \theta_2 \ge (2\pi+\theta_1) \end{Bmatrix} \quad (4)$$

Where θ_1 is the angle of a fixed link, the length R in addition to angles (ψ_1, ψ_2, ψ_3, ψ_4 and γ) can be expressed as follows

Additionally, the angle of the coupler link (θ_3) can be calculated based on Eq. (5) as follows:

$$\theta_3 = \begin{Bmatrix} \psi_2+\psi_4+\theta_2-\pi\,,\ where\quad \theta_1 \le \theta_2 < (\pi+\theta_1) \\ \psi_4-\psi_2+\theta_2-\pi\,,\ where\quad (\pi+\theta_1) \ge \theta_2 \ge (2\pi+\theta_1) \end{Bmatrix} \quad (5)$$

$$\left.\begin{aligned} R &= \sqrt{R_1^2 + R_2^2 - 2R_1R_2\cos\theta_2} \\ \psi_1 &= \cos^{-1}\left[\tfrac{R_1^2+R^2-R_2^2}{2R_1R}\right] \\ \psi_2 &= \cos^{-1}\left[\tfrac{R_2^2+R^2-R_1^2}{2R_2R}\right] \\ \psi_3 &= \cos^{-1}\left[\tfrac{R_4^2+R^2-R_3^2}{2R_4R}\right] \\ \psi_4 &= \cos^{-1}\left[\tfrac{R_3^2+R^2-R_4^2}{2R_3R}\right] \\ \gamma &= \cos^{-1}\left[\tfrac{R_3^2-R^2+R_4^2}{2R_3R_4}\right] \end{aligned}\right\} \quad (6)$$

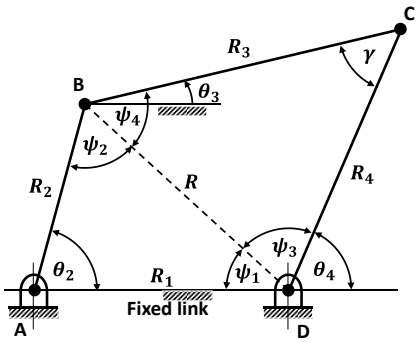

Figure 3- Geometry of Crank-Rocker Mechanism

Undoubtedly, the angular velocity (ω_4) and the angular acceleration (α_4) of the rocker link play an important role in mechanisms. By derivation of Eqs. (4) and (5), angular velocity and angular acceleration of the rocker and coupler link can be calculated.

Taking the time derivative of the above equation and then solving for ω_4 and ω_3, we can get

$$\therefore \omega_4 = \frac{\omega_2 R_2\cos\theta_2 + \omega_3 R_3\cos\theta_3}{R_4\cos\theta_4} \quad (7)$$

$$\therefore \omega_3 = \frac{\omega_2 R_2(\sin\theta_2 - \cos\theta_2\tan\theta_4)}{R_3(\cos\theta_3\tan\theta_4 - \sin\theta_3)} \quad (8)$$

Again, taking the time derivative of the above equations, we have angular accelerations as:

$$\alpha_4 = [\alpha_2 R_2\cos(\theta_2) - \omega_2^2 R_2\sin(\theta_2) - \omega_3^2 R_3\sin(\theta_3) + \omega_4^2 R_4\sin(\theta_4) + \alpha_3 R_3\cos(\theta_3)]/[R_4\cos(\theta_4)] \quad (9)$$

$$\alpha_3 = [\omega_2^2 R_2\cos(\theta_2 - \theta_4) - \omega_4^2 R_4 - \alpha_2 R_2\sin(\theta_4 - \theta_2) + \omega_3^2 R_3\cos(\theta_3 - \theta_4)]/[R_3\sin(\theta_4 - \theta_3)] \quad (10)$$

2.3 Design Techniques for Choosing Transmission Angle Ranges

As reported in [17], the transmission angle γ can be considered the optimal angle if its max-mini values are equally around 90°. Thus, a simple design technique can be used to select the desired range of transmission angle γ based on a previous sense of the max-mini of the angle γ discussed in [19]. In order to apply this method, the summation of γ_{max} and γ_{min} is equal to π. Therefore, the summation of $\cos\gamma_{min}$ and $\cos\gamma_{max}$ is equal to zero accordingly.

$$L_4^2 + L_3^2 - L_2^2 = 1 \quad (11)$$

Where ratios L_2, L_3 and L_4 can be expressed as follows:

$$\left.\begin{aligned} L_2 &= R_2/R_1 \\ L_3 &= R_3/R_1 \\ L_4 &= R_4/R_1 \end{aligned}\right\} \quad (12)$$

Since only two values need to be selected in order to select the range of angles, this technique is relatively simple to use. The first is the intended rocker link angle, θ_{4i}, which is connected to the smallest transmission angle, $\theta_2 = 0$. The second is the preferred transmission angle range ($\gamma = 90^o \pm \delta$), where the angle δ can be chosen.

Two triangles with the limitations of the transmission angle can be solved using the sine rule [20], (Fig. 2), as follows:

$$\frac{L_3}{\sin\theta_{4i}} = \frac{1-L_2}{\sin\gamma_{min}} = \frac{L_4}{\sin(\theta_{4i}-\gamma_{min})} \quad (13)$$

As a result, the prior equation can be rewritten by the following two new inferred equations:

$$L_3 = \frac{\sin\theta_{4i}}{\sin\gamma_{min}}(1 - L_2) \quad (14)$$

$$L_4 = \frac{\sin(\theta_{4i}-\gamma_{min})}{\sin\gamma_{min}}(1 - L_2) \quad (15)$$

In order to write Eq. (11) in a new form, we have to substitute L_3 and L_4 in the elements of the two previous equations as follows:

$$[\mathcal{M}^2 + \mathcal{N}^2 - 1]L_2^2 - 2[\mathcal{M}^2 + \mathcal{N}^2]L_2 + [\mathcal{M}^2 + \mathcal{N}^2 - 1] = 0 \quad (16)$$

Where:

$$\mathcal{M} = \frac{\sin\theta_{4i}}{\sin\gamma_{min}} \quad \text{and} \quad \mathcal{N} = \frac{\sin(\theta_{4i}-\gamma_{min})}{\sin\gamma_{min}}$$

Therefore;

$$L_2 = \frac{\mathcal{M}^2+\mathcal{N}^2}{\mathcal{M}^2+\mathcal{N}^2-1} - \frac{\sqrt{2\mathcal{M}^2+2\mathcal{N}^2-1}}{\mathcal{M}^2+\mathcal{N}^2-1} \quad (17)$$

The plus sign was disregarded in the preceding square root since the value $(\mathcal{M}^2 + \mathcal{N}^2)/(\mathcal{M}^2 + \mathcal{N}^2 - 1)$ is always greater than one. Additionally, L_2 is never greater than one due to the crank-rocker mechanism's shorter links than their set length.

In the meantime, it is possible to determine the values of L_2, L_3, and L_4 by choosing the desired values of θ_{4i} of the rocker links in addition to the available transmission angle range ($\gamma = 90^o \pm \delta$).

The transmission angle is not significant based on its absolute value but rather on its deviation from 90˚. There are different limits suggested for transmission angles are 35-145˚, 40-140˚, and 45-135˚ [25].

3. Mathematical Formulation

3.1 Laminated Composite Links

A rectangular laminated composite link with N orthotropic layers is shown in Fig. 4. This link is in a cartesian coordinate system (x, y, z) whose origin is "0". We chose to use the undeformed middle composite link in the laminate as the x-y plane. A positive z-axis is chosen for the midplane going downward. The thickness of the links is indicated by the letter "h". Link dimensions in the x and y directions are indicated by 'a' and 'b', respectively. There is perfect bonding between orthotropic layers and temperature-independent mechanical properties.

According to Reddy [26] third-order shear deformation theory, the displacements of a point in the plate that is z distances from the reference plane are given by

$$\left.\begin{aligned} u(x,y,z) &= u_0(x,y) + z\Omega_x(x,y) + \tfrac{4}{3h^2}z^3\left(\Omega_x(x,y) + \tfrac{\partial w_0}{\partial x}\right) \\ v(x,y,z) &= v_0(x,y) + z\Omega_y(x,y) + \tfrac{4}{3h^2}z^3\left(\Omega_y(x,y) + \tfrac{\partial w_0}{\partial y}\right) \end{aligned}\right\} \quad (18)$$

$$w(x,y,z) = w_0(x,y)$$

Where u_0, v_0 are in-plane displacements, whereas w_0 denotes the transverse displacement of any point in the midplane, and w, u, and v are the displacement components of any point in the laminate element in the z, x, and y directions, respectively. Additionally, Ω_x and Ω_y are rotations of lines that were originally normal to the center plane about the x and y axes. It is possible to express the in-plain strain vector $\epsilon = [\epsilon_x \epsilon_y \tau_{xy}]^T$ as follows:

$$\epsilon = \epsilon_0 + z\Re_1 + z^3\Re_2 \quad (19)$$

Where:

$$\left.\begin{aligned} \epsilon_0 &= \begin{bmatrix} \frac{\partial u_0}{\partial x} \\ \frac{\eth v_0}{\partial y} \\ \frac{\partial u_0}{\partial y} + \frac{\partial v_0}{\partial x} \end{bmatrix} \\ \Re_1 &= \begin{bmatrix} \frac{\partial \Omega_x}{\partial x} \\ \frac{\eth \Omega_y}{\partial y} \\ \frac{\partial \Omega_x}{\partial y} + \frac{\partial \Omega_y}{\partial x} \end{bmatrix} \\ \Re_2 &= \frac{4}{3h^2}\begin{bmatrix} \frac{\partial \Omega_x}{\partial x} + \frac{\partial \theta_x}{\partial x} \\ \frac{\partial \Omega_y}{\partial y} + \frac{\partial \theta_y}{\partial y} \\ \frac{\partial \Omega_x}{\partial x} + \frac{\partial \Omega_y}{\partial y} + \frac{\partial \theta_y}{\partial y} + \frac{\partial \theta_y}{\partial y} \end{bmatrix} \end{aligned}\right\} \quad (20)$$

The derivative of w_0 concerning **x** and **y** are $\theta_x = \partial w_0/\partial x$ and $\theta_y = \partial w0/\partial y$.

Vector of transverse shear strain $\tau = [\tau_{xz}\tau_{yz}]^T$ has the following form:

$$\tau = \epsilon_s + z^2\Re_s \quad (21)$$

Where:

$$\epsilon_s = \begin{bmatrix} \Omega_x + \frac{\partial w_0}{\partial x} \\ \Omega_y + \frac{\partial w_0}{\partial y} \end{bmatrix}, \quad \Re_s = \frac{4}{h^2}\begin{bmatrix} \Omega_x + \theta_x \\ \Omega_y + \theta_y \end{bmatrix} \quad (22)$$

The shear strains, so that the shear stresses, follow a quadratic pattern, as shown in Eq. (21). Hooke's law of plane stress can be used to obtain the constitutive equation for an orthotropic layer in the local coordinate system by:

$$\begin{Bmatrix} \sigma_1 \\ \sigma_2 \\ \lambda_{12} \\ \lambda_{13} \\ \lambda_{23} \end{Bmatrix} = \begin{bmatrix} U_{11} & U_{12} & 0 & 0 & 0 \\ U_{12} & U_{22} & 0 & 0 & 0 \\ 0 & 0 & U_{33} & 0 & 0 \\ 0 & 0 & 0 & U_{44} & 0 \\ 0 & 0 & 0 & 0 & U_{55} \end{bmatrix} \begin{Bmatrix} \epsilon_1 \\ \epsilon_2 \\ \tau_{12} \\ \tau_{13} \\ \tau_{23} \end{Bmatrix} \quad (23)$$

It is possible to write U_{ij} in the matrix [U] as engineering constants based on the layer material axes.

$$\left.\begin{aligned} U_{11} &= \frac{E_1}{1 - v_{12}v_{21}} & U_{33} &= G_{12} \\ U_{12} &= \frac{v_{12}E_2}{1 - v_{12}v_{21}} & U_{44} &= G_{13} \\ U_{22} &= \frac{E_2}{1 - v_{12}v_{21}} & U_{55} &= G_{23}, \quad \frac{v_{12}}{E_1} = \frac{v_{21}}{E_2} \end{aligned}\right\} \quad (24)$$

Where G_{12}, G_{13}, and G_{23} are the shear modulus, while E_1 and E_2 are the Young modulus, and v_{12} and v_{21} are Poisson's ratios. In general, orthotropic laminates consist of several layers, and the laminate coordinate system (x, y, z) should be translated into the material axis system of Eq (23). Therefore, the stress-strain equation might be written as follows:

$$\begin{Bmatrix} \sigma_x \\ \sigma_y \\ \lambda_{xy} \\ \lambda_{xz} \\ \lambda_{yz} \end{Bmatrix} = \begin{bmatrix} \mathfrak{D}_{11} & \mathfrak{D}_{12} & \mathfrak{D}_{13} & 0 & 0 \\ \mathfrak{D}_{12} & \mathfrak{D}_{22} & \mathfrak{D}_{23} & 0 & 0 \\ \mathfrak{D}_{13} & \mathfrak{D}_{23} & \mathfrak{D}_{33} & 0 & 0 \\ 0 & 0 & 0 & \mathfrak{D}_{44} & \mathfrak{D}_{45} \\ 0 & 0 & 0 & \mathfrak{D}_{45} & \mathfrak{D}_{55} \end{bmatrix} \begin{Bmatrix} \epsilon_x \\ \epsilon_y \\ \tau_{xy} \\ \tau_{xz} \\ \tau_{yz} \end{Bmatrix} \quad (25)$$

Where $\mathfrak{D}_{ij}$ stands for the lamina's converted material constants ($c = cos\ \varphi,\ s = sin\ \varphi$).

$$\left.\begin{aligned} \mathfrak{D}_{11} &= U_{11}c^4 + (2U_{11} + 4U_{33})c^2s^2 + U_{22}s^4 \\ \mathfrak{D}_{12} &= U_{12}c^4 + U_{12}s^4 + (U_{11} + U_{22} - 4U_{33})c^2s^2 \\ \mathfrak{D}_{22} &= U_{11}s^4 + (2U_{12} + 4U_{33})c^2s^2 + U_{22}c^4 \\ \mathfrak{D}_{13} &= (U_{11} - U_{12} - 2U_{33})c^3s + (U_{12} - U_{22} - 2U_{33})s^3c \\ \mathfrak{D}_{23} &= (U_{11} - U_{12} - 2U_{33})s^3c + (U_{12} - U_{22} + 2U_{33})c^3s \\ \mathfrak{D}_{33} &= U_{33}c^4 + U_{33}s^4 + (U_{11} + U_{22} - 2U_{12} - 2U_{33})c^2s^2 \\ \mathfrak{D}_{44} &= U_{44}c^2 + U_{55}s^2 \\ \mathfrak{D}_{45} &= U_{55}cs - U_{44}cs \\ \mathfrak{D}_{55} &= U_{55}c^2 + U_{44}s^2 \end{aligned}\right\} \quad (26)$$

As a result of deformation, the material obtains a strain energy consisting of the total energy resulting from bending and shearing deformation, which can be calculated as follows:

$$\mathfrak{T} = \frac{1}{2}\int_A \sum_{l=1}^{NL}\int_{zl-1}^{zl}\{\tau\}^T[Q]_l\{\tau\}dzdA + \frac{1}{2}\int_A \sum_{l=1}^{NL}\int_{zl-1}^{zl}\{\epsilon\}^T[Q]_l\{\epsilon\}dzdA \quad (27)$$

Equations (19) and (21) can be substituted for Eq. (27) and integrated in terms of z to obtain

$$[\mathfrak{T}] = \frac{1}{2}\int_A \{\epsilon_0\}^T[\mathfrak{H}]\{\epsilon_0\} + \{\epsilon_0\}^T[\mathfrak{B}]\{\mathfrak{R}_1\} + \{\epsilon_0\}^T[\Lambda]\{\mathfrak{R}_2\} + \{\mathfrak{R}_1\}^T[\mathfrak{B}]\{\epsilon_0\} + \{\mathfrak{R}_1\}^T[\mathfrak{L}]\{\mathfrak{R}_1\} + \{\mathfrak{R}_1\}^T[\mathfrak{f}]\{\mathfrak{R}_2\} + \{\mathfrak{R}_2\}^T[\Lambda]\{\epsilon_0\} + \{\mathfrak{R}_2\}^T[\mathfrak{f}]\{\mathfrak{R}_1\} + \{\mathfrak{R}_2\}^T[\mathfrak{A}]\{\mathfrak{R}_2\}\,dA + \frac{1}{2}\int_A \{\epsilon_s\}^T[\mathfrak{H}_s]\{\epsilon_s\} + \{\epsilon_s\}^T[\mathfrak{L}_s]\{\mathfrak{R}_s\} + \{\mathfrak{R}_s\}^T[\mathfrak{L}_s]\{\epsilon_s\} + \{\mathfrak{R}_s\}^T[\mathfrak{f}_s]\{\mathfrak{R}_s\}\,dA \quad (28)$$

Where:

$$\left.\begin{aligned}
[\mathfrak{H}] &= \sum_{l=1}^{NL}\left[\mathcal{Q}_b\right]_l(z_l - z_{l-1})\\
[\mathfrak{B}] &= \frac{1}{2}\sum_{l=1}^{NL}\left[\mathcal{Q}_b\right]_l(z_l^2 - z_{l-1}^2)\\
[\mathfrak{L}] &= \frac{1}{3}\sum_{l=1}^{NL}\left[\mathcal{Q}_b\right]_l(z_l^3 - z_{l-1}^3)\\
[\Lambda] &= \frac{1}{4}\sum_{l=1}^{NL}\left[\mathcal{Q}_b\right]_l(z_l^4 - z_{l-1}^4)\\
[\mathfrak{f}] &= \frac{1}{5}\sum_{l=1}^{NL}\left[\mathcal{Q}_b\right]_l(z_l^5 - z_{l-1}^5)\\
[\mathfrak{A}] &= \frac{1}{7}\sum_{l=1}^{NL}\left[\mathcal{Q}_b\right]_l(z_l^7 - z_{l-1}^7)\\
\left[\mathfrak{H}_s\right] &= \sum_{l=1}^{NL}\left[\mathcal{Q}_s\right]_l(z_l - z_{l-1})\\
[\mathfrak{L}_s] &= \frac{1}{3}\sum_{l=1}^{NL}\left[\mathcal{Q}_s\right]_l(z_l^3 - z_{l-1}^3)\\
\left[\mathfrak{f}_s\right] &= \frac{1}{5}\sum_{l=1}^{NL}\left[\mathcal{Q}_s\right]_l(z_l^5 - z_{l-1}^5)
\end{aligned}\right\} \quad (29)$$

Moreover, it is possible to simplify Eq. (28) as follows:

$$\mathfrak{T} = \frac{1}{2}\{D\}^T\left\{\int_A\left[[B]^T[\overline{D}][B] + [B_S]^T[D_S][B_S]\right]dA\right\}\{D\} \quad (30)$$

Where, $[D_S]$ and $[\overline{D}]$ are matrices of material constants given by

$$[D_S] = \begin{bmatrix}\mathfrak{H}_s & \mathfrak{L}_s\\ \mathfrak{L}_s & \mathfrak{f}_s\end{bmatrix}, \quad [\overline{D}] = \begin{bmatrix}\mathfrak{H} & \mathfrak{B} & \Lambda\\ \mathfrak{B} & \mathfrak{L} & \mathfrak{f}\\ \Lambda & \mathfrak{f} & \mathfrak{A}\end{bmatrix} \quad (31)$$

The global stiffness matrix $[k]$ of the element is given by the area integral in Eq. (30), which can be expressed as follows:

$$[k] = \int_A\left[[B]^T[\overline{D}][B] + [B_S]^T[D_S][B_S]\right]dA \quad (32)$$

Based on the stiffness matrix, we can express strain energy as

$$[\mathfrak{T}] = \frac{1}{2}[D]^T[k][D] \quad (33)$$

Remembering the definitions of ϵ_0, $\mathfrak{R}_1$, $\mathfrak{R}_2$, ϵ_s, and $\mathfrak{R}_s$, see Eqs. (20) and (21), we can write them by the following formula:

$$\begin{Bmatrix}\epsilon_0\\ \mathfrak{R}_1\\ \mathfrak{R}_2\end{Bmatrix} = \left[\wp_1\right]\{\epsilon_{xy}\} \quad (34)$$

$$\begin{Bmatrix}\epsilon_0\\ \mathfrak{R}_s\end{Bmatrix} = [\mathfrak{X}_1]\{\tau_{xy}\} \quad (35)$$

Where:

$$\{\epsilon_{xy}\} = \{u_{0,x}u_{0,y}v_{0,x}v_{0,y}\phi_{x,x}\phi_{x,y}\phi_{y,x}\phi_{y,y}\Theta_{x,x}\Theta_{x,y}\Theta_{y,x}\Theta_{y,y}\} \quad (36)$$

$$\{\tau_{xy}\} = \{w_{0,x}w_{0,y}\phi_x\phi_y\Theta_x\Theta_y\} \quad (37)$$

The derivatives connected to ***s*** and ***t*** must then be used to write $\{\epsilon_{xy}\}$ and $\{\tau_{xy}\}$, which are defined based on the derivatives related to ***x*** and ***y***. The Jacobian matrix, $[\mathfrak{W}]$, which is connected to the derivatives of the two coordinate systems, can be used to achieve this if it is defined as follows:

$$[T] = [\mathfrak{W}]^{-1} = \frac{1}{[\mathfrak{W}]}\begin{bmatrix}\partial y/\partial t & -\partial y/\partial s\\ -\partial x/\partial t & \partial y/\partial s\end{bmatrix} \quad (38)$$

This can be written as follows:

$$\{\epsilon_{xy}\} = \begin{bmatrix}T & 0 & 0 & 0 & .\\ 0 & T & 0 & 0 & .\\ 0 & 0 & T & 0 & .\\ 0 & 0 & 0 & T & .\\ . & . & . & . & .\end{bmatrix}\begin{Bmatrix}u_{0,S}\\ u_{0,t}\\ v_{0,s}\\ .\\ .\end{Bmatrix} = \left[\wp_2\right]\{\epsilon_{st}\} \quad (39)$$

And

$$\{\tau_{xy}\} = \begin{bmatrix}T & 0\\ 0 & I\end{bmatrix}\{\tau_{st}\} = [\mathfrak{X}_2]\{\tau_{st}\} \quad (40)$$

Where $[I]$ is the identity matrix.

$$\left.\begin{aligned}\{\epsilon_{st}\} &= \left[\wp_3\right]\{D\}\\ \{\tau_{st}\} &= [\mathfrak{X}_3]\{D\}\end{aligned}\right\} \quad (41)$$

Where $\left[\wp_1\right]$, $\left[\wp_2\right]$, $\left[\wp_3\right]$, $[\mathfrak{X}_1]$, and $[\mathfrak{X}_2]$ and $[\mathfrak{X}_3]$ are defined in [30]. The following equation is obtained by representing the $\{\epsilon\}$ and $\{\tau\}$ in the final stage as nodal degrees of freedom.

$$\left.\begin{aligned}[B] &= \left[\wp_1\right]\left[\wp_2\right]\left[\wp_3\right]\\ [B_s] &= [\mathfrak{X}_1]\,[\mathfrak{X}_2][\mathfrak{X}_3]\end{aligned}\right\} \quad (42)$$

The kinetic energy expression is used to obtain the mass matrix for the dynamic analysis of laminated composite links.

$$[\mathcal{T}] = \frac{1}{2}\int_A \sum_{j=1}^{n}\int_{z_{j-1}}^{z_j}\rho_j\{\dot{u}^2 + \dot{v}^2 + \dot{w}^2\}dzdA \quad (43)$$

By replacing the time derivatives of the displacements in Eq. (18) into Eq. (43), we can obtain

$$[\mathcal{T}] = \frac{1}{2}\int_A \sum_{j=1}^{n}\int_{z_{j-1}}^{z_j} \rho_j \{(\dot{u}_0^2 + \dot{v}_0^2 + \dot{w}_0^2) + (z^2 + 2cz^4 + c^2z^6)(\dot{\phi}_x^2 + \dot{\phi}_y^2) + c^2z^6(\dot{\Theta}_x^2 + \dot{\Theta}_y^2) + 2(z + cz^3)(\dot{\phi}_x\dot{u}_0 + \dot{\phi}_y\dot{v}_0) + 2cz^3(\dot{\Theta}_x\dot{u}_0 + \dot{\Theta}_y\dot{v}_0) + 2(cz^4 + c^2z^6)(\dot{\phi}_x\dot{\Theta}_x + \dot{\phi}_y\dot{\Theta}_y)\}dzdA \quad (44)$$

It is logical to assume that displacements are time-dependent harmonic functions. Thus, everyone can be pre-multiplied by $e^{i\omega t}$. To help define the mass matrix, if the expressions defined in [29] are substituted in Eq. (43), and the integration is performed in the z-direction, the following equation is obtained.

$$[\mathcal{T}] = \frac{1}{2}\omega^2 \int_A \{d\}^T \sum_{j=1}^{n}\int_{z_{j-1}}^{z_j} \rho_j \{[\Delta_1 + g_1[\Delta_2] + g_2[\Delta_3] + g_3[\Delta_4] + g_4[\Delta_5] + g_5[\Delta_6]]\}dzdA \quad (45)$$

Where: $[\Delta_i]$ and $g_i$are defined in the [31], $\{d\}$ is the continuum displacement vector, $\{d\} = \{u\ v\ w\ \phi_x\ \phi_y \Theta_x\ \Theta_y\}$.

Eq. (32) can be rewritten in the shortened form as follows:

$$[\mathcal{T}] = \frac{1}{2}\omega^2\{D\}^T[m]\{D\} \quad (46)$$

Where: [**m**] is the element mass matrix

3.2 Finite Element Model of Four Bar Mechanism

The finite element method FEM is a powerful numerical technique using variational and interpolation methods to model and solve boundary value problems. The FEM of four bar planar mechanism with three beam elements is shown in Fig. 4. In this figure, it is seen that each link is modeled by one finite beam element. The figure also contains three elements and 8 nodes; each node has three degrees of freedom, translational motions in the nodal of the x-axis and the y-axis direction, and a rotational motion around the z-axis. The translation motions at node 1 and node 8 are equal to zero because they are connected to the fixed link.

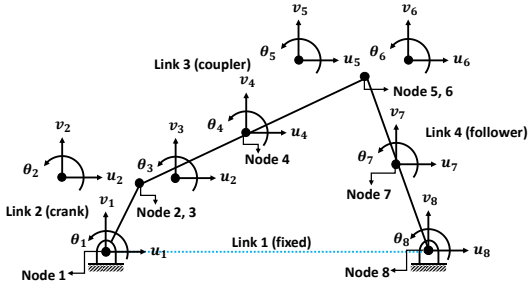

Figure 4- Finite Element Model of Four Bar Mechanism.

The strain (potential) energy and kinetic energy of one beam element (one link) in matrix form are explained by Eqs. (29) and (42), respectively.

Where $[m]$ is the mass matrix, which can be given as [29]:

$$[m] = \rho AL\begin{bmatrix} 1/3 & 0 & 0 & 1/6 & 0 & 0 \\ 0 & 13/35 & 11L/210 & 0 & 9/70 & -13L/420 \\ 0 & 11L/210 & L^2/105 & 0 & 13L/420 & -L^2/140 \\ 1/6 & 0 & 0 & 1/3 & 0 & 0 \\ 0 & 9/70 & 13L/420 & 0 & 13/35 & -11L/210 \\ 0 & -13L/420 & -L^2/140 & 0 & -11L/210 & L^2/105 \end{bmatrix} \quad (43)$$

The stiffness matrix, [k], is formed as [27]:

$$[k] = \begin{bmatrix} EA/L & 0 & 0 & -EA/L & 0 & 0 \\ 0 & 12EI/L^3 & 6EI/L^2 & 0 & -12EI/L^3 & 6EI/L^2 \\ 0 & 6EI/L^2 & 4\,EI/L & 0 & -6EI/L^2 & -2\,EI/L \\ -EA/L & 0 & 0 & EA/L & 0 & 0 \\ 0 & -12EI/L^3 & -6EI/L^2 & 0 & 12EI/L^3 & -6EI/L^2 \\ 0 & 6EI/L^2 & 2\,EI/L & 0 & -6EI/L^2 & 4\,EI/L \end{bmatrix} \quad (44)$$

The total mass and stiffness matrix of the four-bar mechanism is given by

$$[M] = [A]^T[m][A] \quad (45)$$

$$[K] = [A]^T[k][A] \quad (46)$$

where $[A]$ is the transformation matrix.

$$[A] = \begin{bmatrix} \delta & \mu & 0 & 0 & 0 & 0 \\ -\mu & \delta & 0 & 0 & 0 & 0 \\ 0 & 0 & 1 & 0 & 0 & 0 \\ 0 & 0 & 0 & \delta & \mu & 0 \\ 0 & 0 & 0 & -\mu & \delta & 0 \\ 0 & 0 & 0 & 0 & 0 & 1 \end{bmatrix} \quad (47)$$

Where $\delta = \cos\theta : \mu = \sin\theta$, and θ is the orientation of the element regarding the global coordinate system.

From the free vibration of the system, the equation of motion for the mechanism may be written in matrix form, as described in Eq. (48)

$$[M]\{\ddot{U}\} + [K]\{U\} = \{0\} \quad (48)$$

From the following equation, the natural frequencies and modal vectors can be obtained for the four-bar mechanism:

$$|[K] - \eta_i[M]|\{V_i\} = \{0\} \quad (49)$$

$$(i = 1.2.3, \ldots\ldots, n)$$

Where $\eta_i = \omega_i^2$ and $\{V_i\}$ are the eigenvalues and eigenvectors of the four-bar mechanism model, respectively. By solving Eq. (49) using MATLAB software, we can obtain the eigenvalue and eigenvector [30].

4. Experimental Procedure

Glass fibers and carbon fibers were used in the fabrication of the prototype of the composite linkage, along with polyester as the matrix for the composite along with catalyst as the reinforcing element. The laminated hybrid and nonhybrid composite beam links of CR mechanisms, which have a fiber volume percentage of 60%, are reinforced using the same five layers of glass and carbon fiber. The links were cut to the required dimensions using a fine sawtooth, as shown in Fig. 5. [31].

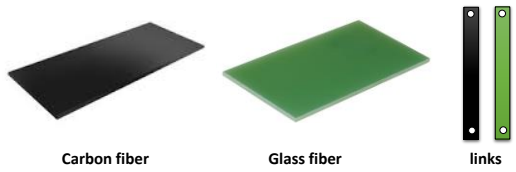

Figure 5 - Composite CR Mechanism Linkages.

4.1 Experimental testing

The CR mechanisms of composite links were tested in four cases. Their linkage proportions are listed in Table 3 [27].

Table 3. Proportions linkage of (C-R) mechanism

Mechanism	Case-1	Case-2	Case-3	Case-4
R1	1.00	1.00	1.00	1.00
R2	0.27	0.42	0.14	0.21
R3	0.83	1.00	0.90	0.91
R4	0.67	0.79	0.46	0.46

A pulse vibration test equipment was used to conduct vibration tests on the built composite CR mechanism. As seen in Fig. 6(a & b), this test equipment includes a fast Fourier transform (FFT) analyzer (B&K 3560), a computer, a laser vibrometer, and a modal impact hammer (B&K 2302-5). For various mechanisms, the corresponding fundamental frequencies of the prototype are measured and recorded at an angle (= 9045°). With the aid of the impact hammer, the composite mechanism was stimulated at the coupler link's midpoint. Through the laser vibrometer, the samples' vibration responses were recorded. Additionally, using the pulse program and the frequency response function (FRF), the natural frequencies and damping properties were discovered [32]. FRFs were also obtained by hammer impact testing on average three times

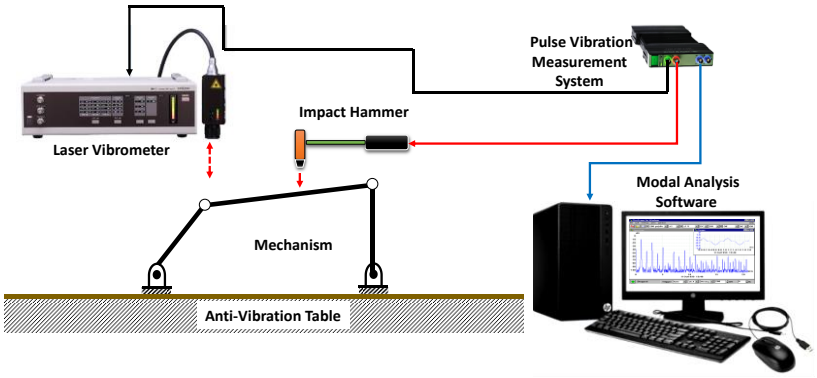

(a): Experimental Layout of this Study.

(b): Diagram of the Measuring System.

Figure 6- A Test Was Conducted Experimentally with a Dual-Channel Analyzer.

5. Results and Discussion

5.1 Transmission Angle Results

In the case of hybrid composite links, we examined four cases related to the CR mechanism. A list of the binding ratios for the four cases is shown in Table 3. Six combinations of hybrid composite materials with three different transmission angles were used. This research mainly aims to improve the dynamic properties of the CR mechanisms and investigate the effect of the transmission angle on the mechanism's dynamic performance.

A mini-max sense of optimal transmission angles was used when selecting case-3 linkages proportions, as well as case-4's linkages proportions. This indicates that the case-3 transmission angle range is $\gamma = 90 \pm 20^{\circ}$. However, the transmission angle's range of case-4 is $\gamma = 90 \pm 30^{\circ}$. Furthermore, the CR mechanism's linkages proportions of case-1, in addition to CR mechanism's linkages proportions of case-2, were selected as general CR mechanisms where transmission angle's limits of case-1 are $\gamma_{max} = 115.35^{\circ}$ and $\gamma_{min} = 58.26^{\circ}$ in addition to $\gamma_{max} = 103.95^{\circ}$ and $\gamma_{min} = 35.65^{\circ}$ for case-2.

For various situations with hybrid composite mechanisms, the relationship between the crank angle (θ_2) and the transmission angle (γ) is shown in Fig. 7. The curves show that case-1 and case-4 roughly follow the same trend, and that the range of their transmission angles is equal to or greater than 60°. Case-4 also has the highest transmission angle values, while Case-2 has the lowest transmission angle values.

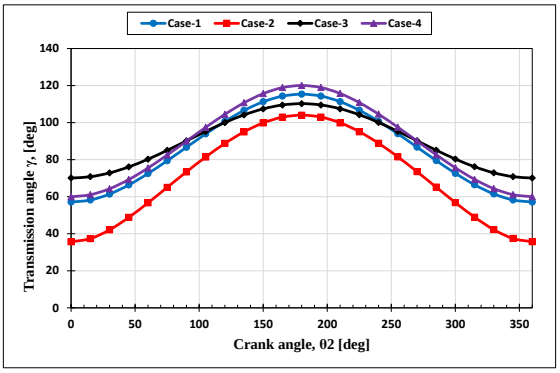

Figure 7- Relationship between Transmission Angle (γ) and Crank Angle (θ_2)

5.2 Dynamic Results

The resonance frequency of the CR mechanism with composite linkages has been recorded with four cases, three types of transmission angles (minimum angle, 90º, and maximum angle), and different types of staking sequences. Tables 4, 5, & 6 show measured and computed fundamental frequencies. Experimental results confirmed the numerical value obtained from Eq. 49. According to the present study, numerical results are remarkably similar to experimental results.

5.2.1 Effect of Laminate Codes on Eigen Frequency

In this paper, six different laminate codes were selected; each with a different stacking sequence from the other. The properties of these cases are summarized in Table 2.

Fig. 8 indicates that the specimen of laminate code [C6] has the lowest frequency compared with the other specimen, while the specimen of laminate code [C1] has the highest values. This is due to the minimum and maximum values of flexural elastic modules and stiffness at these laminate codes, respectively .

Tables 4, 5 & 6 show that the frequency values significantly varied with the state of stacking sequences. This is because the outer staking layer is more effective on stiffness than the inner layer. The change of laminate code from [C1] to [C6] decreases the eigenfrequency by 62.22%.

From Fig. 9, it can be observed that the specimen of laminate code [C1] has the lowest damping factor compared with the other specimen, while the specimen of laminate code [C6] has the highest values, which is due to the minimum and maximum values of flexural elastic modules. Tables 4, 5, & 6 reveal that the change of laminate code from [C1] to [C6] increases the damping factor by 28.63%.

5.2.2 Effect of Cases Type on Eigen Frequency

Four cases are studied to assess the efficacy of the suggested mechanism; each case has different dimensions from the other based on the research [27]. The specifications of these cases are listed in Table 3.

Numerical and experimental results agree with each other in this paper. From Fig.9, it can be noted that the CR mechanism with Case 2 has the lowest frequency compared with the other cases, while the CR mechanism with Case 3 has the highest values. This is due to the highest and lowest value of the stiffness in each case as a result of the change in the dimensions of the mechanism.

In contrast, as shown in Figure 9, the CR mechanism with Case 2 has the highest damping factor among

the other cases, while the CR mechanism with Case 3 has the lowest damping factor. Because of the change in the dimensions of the mechanism, the dissipated energy in each case has the highest and lowest values. According to Tables 4, 5, & 6, the natural fundamental frequencies increased by 41.55

%, and the damping factor decreased by 15.78% when the CR mechanism with composite links was changed from Case 2 to Case 3.

5.2.3 Effect of Transmission Angle on Eigen Frequency

Three types of transmission angles are studied in this paper. The values of these angles have been chosen at: the minimum position, the maximum position, and the 90˚.

Fig 8 illustrates the maximum value of fundamental natural frequency at the maximum position of transmission angle, while the minimum value at the position of 90˚. The maximum value of fundamental natural frequency is at the maximum position of transmission angle, while the minimum value is at the position of 90˚. This is due to the maximum and minimum values of the stiffness at these positions, which means that the best efficiency of the mechanism is when the transmission angle is at or near 90˚.

According to Tables 4, 5, & 6, changing the transmission angle from maximum to minimum value reduces the fundamental frequency by 15.93%. In contrast, by changing the transmission angle from the maximum to 90°, the fundamental frequency is reduced by 26.17%.

Table 4: Fundamental natural frequency in Hz and damping ratio at various types of stacking sequence in four cases of CR mechanism at $\gamma = \min^{o}$.

Laminate Codes	Fundamental natural frequency and damping factor at γ = min											
	Case 1			Case 2			Case 3			Case 4		
	FE	Ex	ξ	FE	Ex	ξ	FE	Ex	ξ	FE	Ex	ξ
C_1	194.1	191.1	0.314	143.7	140.4	0.361	247.1	239.4	0.261	229.2	223.4	0.274
C_2	159.5	155.1	0.341	119.2	115.2	0.381	192.5	189.3	0.316	178.4	175.3	0.322
C_3	132.1	130.1	0.391	101.3	99.07	0.415	152.2	150.4	0.341	139.4	138.5	0.341
C_4	106.3	101.2	0.403	83.14	80.38	0.423	123.3	120.1	0.382	108.3	106.3	0.352
C_5	86.00	85.14	0.418	67.34	66.20	0.433	101.4	99.01	0.417	84.84	82.10	0.371
C_6	68.80	67.42	0.434	55.3	55.39	0.445	84.96	83.09	0.424	66.17	63.23	0.392

Table 5: Fundamental natural frequency in Hz and damping ratio at various types of stacking sequence in four cases of CR mechanism at $\gamma = 90^{o}$.

Laminate Codes	Fundamental natural frequency and damping factor at $\gamma = 90^{o}$											
	Case 1			Case 2			Case 3			Case 4		
	FE	Ex	ξ	FE	Ex	ξ	FE	Ex	ξ	FE	Ex	ξ
C_1	173.2	169.4	0.316	99.34	97.35	0.411	201.2	195.1	0.301	194.1	191.2	0.312
C_2	143.4	142.2	0.378	82.45	79.5	0.422	166.3	164.1	0.322	161.4	156.4	0.324
C_3	122.1	118.3	0.391	70.08	69.33	0.431	141.2	139.1	0.391	136.4	134.1	0.382
C_4	100.1	98.21	0.398	57.47	56.32	0.443	116.2	113.0	0.401	112.2	109.2	0.395
C_5	83.2	82.18	0.411	47.70	47.22	0.454	96.52	94.4	0.421	93.22	91.4	0.422
C_6	67.3	65.90	0.433	38.34	37.51	0.461	78.18	75.3	0.431	75.51	74.1	0.421

Table 6: Fundamental natural frequency in Hz and damping ratio at various types of stacking sequence in four cases of CR mechanism at γ = max.

Laminate Codes	Fundamental natural frequency and damping factor at γ = max											
	Case 1			Case 2			Case 3			Case 4		
	FE	Ex	ξ	FE	Ex	ξ	FE	Ex	ξ	FE	Ex	ξ
C_1	226.1	221.2	0.262	162.2	159.3	0.314	263.3	258.1	0.231	248.4	243.2	0.252
C_2	188.3	185.3	0.284	134.4	131.2	0.363	218.4	213.2	0.271	206.3	201.2	0.281
C_3	160.2	157.2	0.312	114.3	112.3	0.391	186.1	180.2	0.311	175.4	172.1	0.313
C_4	131.3	128.1	0.361	93.12	92.11	0.413	152.3	150.3	0.331	143.4	140.3	0.331
C_5	108.2	107.3	0.371	77.40	75.24	0.421	126.0	123.4	0.362	119.3	117.3	0.351
C_6	88.21	86.21	0.403	63.10	61.14	0.433	102.5	100.2	0.371	96.70	94.21	0.384

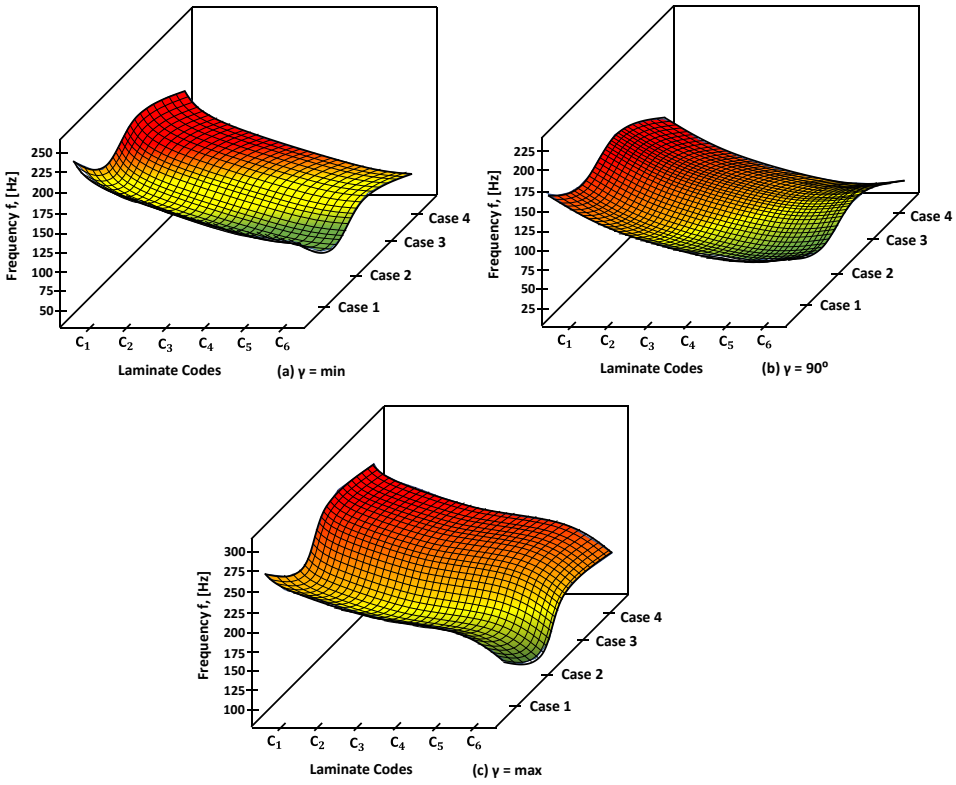

Figure 8 - Fundamental Natural Frequency at Four Cases, Three Types of Transmission Angle and Different Types of Stacking Sequence.

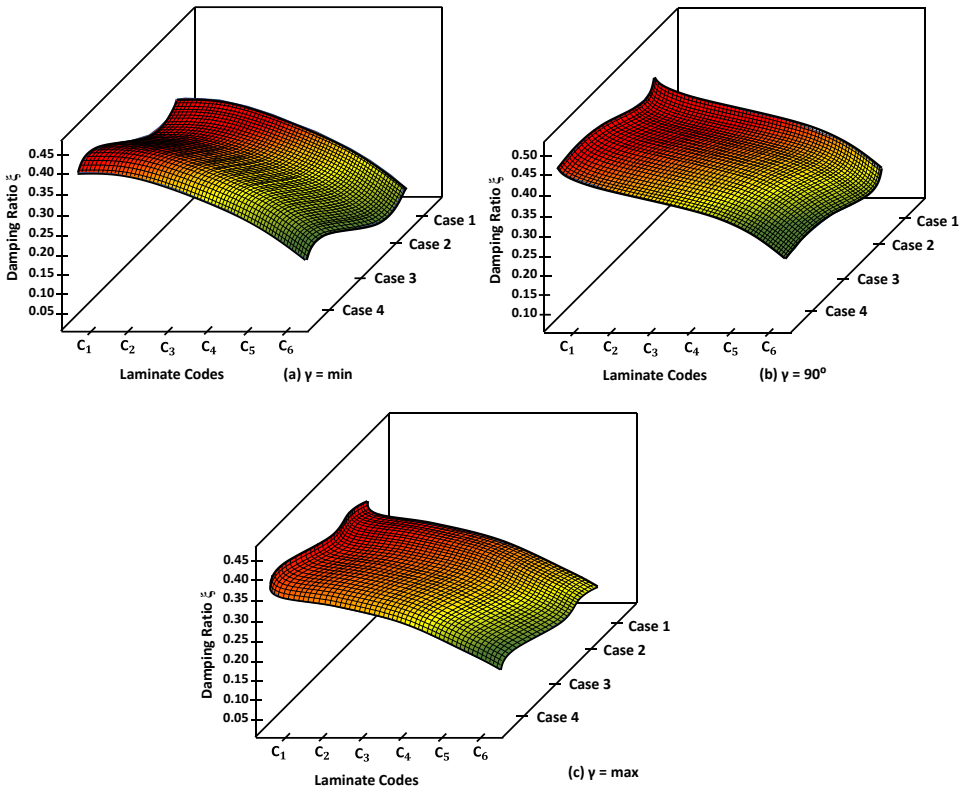

Figure 9 - Damping Ratio at Four Cases, Three Types of Transmission Angle and Different Types of Stacking Sequence.

6. Conclusions

Recently, reducing energy consumption can be considered as one of major concerns for most countries in the world, especially industrial countries. In this regard, most of the countries are doing their best to decrease the greatly depleted energy in operating the mechanical machines using many effective techinques. One of these effective techniques is the usage of strong materials with light weight, especially the reinforced composite materials usage for fabricating the moving components of machines. In accordance with this trend of reducing energy consumption, this research attempted to introduce a study deals with the light hybrid composite materials usage for manufacturing the moving components of machines such as the linkages of Crank-Rocker (CR) mechanism. CR mechanisms are one of the main moving components of mechanical machines. Furthermore, the driving power of mechanical machines can be lowered by selecting the appropriate proportions of link lengths corresponding to the optimum transmission angle.

Mostly, this usage lightweight linkages from hybrid composite materials can improve the required dynamic performance in addition to addressing wear and corrosion problems. Also, the high damping and significant rigidity of composite linkages leads to better mechanism performance. In this regard, a mathematical model created in this study to control the dynamic performance of the mechanism by selecting three different shift angles in addition to four different states of the mechanism.

Based on the results, the CR mechanism performs best at 90° of the transmission angle, as the average natural frequency of this angle decreases by 11.19 % and 26.17 % compared to the maximum and minimum transmission angles. Furthermore, measuring and theoretical fundamental response frequencies of mechanisms are in good agreement.

7. References

[1] J. Brodell, and A. Soni, “Design of the Crank-Rocker Mechanism with Unit Time Ratio”, Journal of Mechanisms, Vol. 5, No. 1, , 1970, pp. 1-4.

[2] R. Singh, H. Chaudhary, and A. Singh, “Defect-free optimal synthesis of crank-rocker linkage using nature-inspired optimization algorithms”, Journal of Mechanism and Machine Theory, Vol. 116, , 2017, pp. 105-122.

[3] A. Hall, in: Kinematic and Linkage Design, Prentice-Hall, Englewood Cliffs, NJ, 1961, pp. 41. (Online).Available:https://babel.hathitrust.org/cgi/pt?id=mdp.39015002035189;view=1up;seq=61 (Accessed: 12- Oct.- 2017).

[4] D. Myszka, in: Machines and Mechanisms: Applied Kinematic Analysis, 4th Edition, Prentice Hall, New York, USA, 2012, pp. 93.

[5] S. Balli and S. Chand, "Transmission Angle in Mechanisms-Triangle in Mech.", Journal of Mechanism and Machine Theory, Vol. 37, No. 2, 2002, pp. 175-195.

[6] K. Waldron, G. Kinzel, and S. Agrrawal, in: Kinematic, Dynamic, and Design of Machinery, Wiley, London, UK, 2016, pp. 102-104. (Online).Available:https://books.google.com.eg/books?id=vRqJCgAAQBAJ&pg=PA102#v=onepage&q&f=false (Accessed: 10- Oct.- 2017).

[7] G. Rothenhofer, C. Walsh, and A. Slocum, "Transmission Ratio Based Analysis and Robust Design of Mechanisms", Journal of Precision Engineering, Vol. 34, 2010, pp. 790-797.

[8] E. Tanik, "Transmission Angle in Complaint Slider-Crank Mechanism", Journal of Mechanism and Machine Theory, Vol. 46, 2011, pp. 1623-1632.

[9] J. Kimberlla, in: Kinematic Analysis and Synthesis, McGraw-Hill, New York, 1991, pp. 14-15. (Online). Available: https://books.google.com.eg/books?hl=ar&id=rBEoAQAAMAAJ (Accessed: 12- Oct.- 2017).

[10] R. Soylu, "Analytical Synthesis of Mechanisms – Part-1", Journal of Mechanism and Machine Theory, Vol. 28, No. 6, 1993, pp. 825-833.

[11] P. Eschenbach and D. Tesar, "Link Length Bounds on the Four Bar Chain", Journal of Engineering for Industry Trans. ASME, Vol. 93, No. 1, 1971, pp. 287-293.

[12] D. Tao, in: Applied Linkage Synthesis, Addison-Wesley, Reading, MA, 1964, pp. 7-12.

[13] P. Rao, "Kinematic Synthesis of Variable Crank-rocker and Drag linkage planar type Five-Bar Mechanisms with Transmission Angle Control", Journal of Engineering Research and Application, Vol. 3, No. 1, 2013, pp. 1246-1257.

[14] T. Patal, "Synthesis of Four Bar Mechanism for Polynomial Function Generation by Complex Algebra", in National Conference in Recent Trends in Engineering & Technology, B.V.M Engineering Collage, Nagar Gujarat INDIA, May 2011, pp. 1-5.

[15] G. Hassaan, "Synthesis of Planar Mechanisms, Part III: Four-Bar Mechanisms for Three Coupler-Positions Generation", Global Journal of Advanced Research, Vol. 2, No. 4, 2015, pp. 726-734.

[16] G. Marín, F. Alonso and M. Castillio, "Shape Optimization for Path Synthesis of Crank-Rocker Mechanisms Using a Wavelet-Based Neural Network", Journal of Mechanism and Machine Theory, Vol. 44, No. 6, 2009, pp. 1132-1143.

[17] K. Gupta, "Design of Four-Bar Function Generators with Mini-Max Transmission Angle", Journal of Engineering for Industry Trans. ASME, Vol. 99, No. 2, 1977, pp. 360-366.

[18] K. Khader, "Nomograms for Synthesizing Crank Rocker Mechanism with a Desired Optimum Range of Transmission Angle", International Journal of Mining, Metallurgy and Mechanical Engineering (IJMMME), Vol. 3, No. 3, 2015, pp. 155-160.

[19] K. Khader, "Computer Aided Design for Synthesizing Mechanism with Optimal Transmission Angle", In: the 6th International Conference on Trends in Mechanical and Industrial Engineering (ICTMIE'2015), Dubai, UAE, Sept., 2015, pp. 12-17.

[20] J. Buśkiewicz, "A Specific Problem of Mechanism Synthesis", Journal of Applied Mechanics and Engineering, Vol. 19, No. 3, 2014, pp. 513-522.

[21] S. Khan, A. Jamal, S. Ali, M. M. Horoub, A. Albalasie and S. Ali, "Dynamic modeling and analysis of a four-bar mechanism for automobile applications", Proc. of the 2nd International Conference on Electrical, Communication and Computer Engineering (ICECCE) 12-13 June 2020, Istanbul, Turkey.

[22] M. Arda, "Dynamic analysis of a four-bar linkage mechanism", International Scientific Journal "Machines Technologies Materials", Vol. 1, No 5, 2020, pp. 186-190.

[23] M. Khorshidi, M. Soheilypour, M. Peyro, A. Atai, M. Shariat Panahi, "Optimal design of four-bar mechanisms using a hybrid multi-objective GA with adaptive local search", Mechanism and Machine Theory, Vol. 46, No 10, 2011, pp. 1453-1465.

[24] P.K. Mallick, "Fiber Reinforced Composites Materials, Manufacturing, and Design," by Taylor & Francis Group, LLC, 2008.

[25] S. Shrinivas Balli and S. Chand, "Transmission Angle in Mechanisms (Triangle in Mech)", Mechanism and Machine Theory, Vol. 37, 2002, pp. 175-195.

[26] J.T. Kimbrella, in: Kinematics Analysis and Synthesis, McGraw-Hill, New York, 1991, pp. 14-15.

[27] K. M. Khader, and M. I. Elimy, "Power and Wear Reduction Using Composite Links of Crank-Rocker Mechanism with Optimum Transmission Angle", World Academy of Science, Engineering and Technology, International Journal of Civil and Environmental Engineering Vol. 12, No 1, 2018, pp. 42-48.

[28] K. Khader, "Computer Aided Design for Synthesizing Mechanism with Optimal Transmission Angle", In: the 6th International Conference on Trends in Mechanical and Industrial Engineering (ICTMIE'2015), Dubai, UAE, Sept., 2015, pp. 12-17.

[29] H. Ouyang, D. Richiedei, and A. Trevisan, "Pole assignment for control of flexible link mechanisms", Journal of Sound and Vibration, Vol. 332, 2013, pp. 2884–2899.

[30] M. Yaman, and M. F. S¸ansveren, "Numerical and experimental vibration analysis of different types of adhesively bonded joints", Structures, Vol. 34, 2021, pp. 368–380.

[31] Reddy JN, "Mechanics of Laminated Composite Plates and Shells: Theory and Analysis", Second Edition-CRC Press 2003.

[32] M. I. Elamy, "Dynamic Analysis of Rotating Continuous Drive Friction Welding Joints of Al alloy (6061AA)", ERJ, Engineering Research Journal, Faculty of Engineering, Menoufia University, Vol. 64, No 1, 2023, pp. 43-53.